Heliyon

Received:
17 November 2017
Revised:
8 January 2018
Accepted:
22 February 2018

Cite as: Ryosuke Matsuzaki, Takeshi Tachikawa, Junya Ishizuka. Estimation of state and material properties during heat-curing molding of composite materials using data assimilation: A numerical study.
Heliyon 4 (2018) e00554.
doi: 10.1016/j.heliyon.2018.e00554

Estimation of state and material properties during heat-curing molding of composite materials using data assimilation: A numerical study

Ryosuke Matsuzaki*, Takeshi Tachikawa, Junya Ishizuka

Department of Mechanical Engineering, Tokyo University of Science, 2641 Yamazaki, Noda, Chiba 278-8510, Japan

* Corresponding author.

E-mail address: rmatsuza@rs.tus.ac.jp (R. Matsuzaki).

Abstract

Accurate simulations of carbon fiber-reinforced plastic (CFRP) molding are vital for the development of high-quality products. However, such simulations are challenging and previous attempts to improve the accuracy of simulations by incorporating the data acquired from mold monitoring have not been completely successful. Therefore, in the present study, we developed a method to accurately predict various CFRP thermoset molding characteristics based on data assimilation, a process that combines theoretical and experimental values. The degree of cure as well as temperature and thermal conductivity distributions during the molding process were estimated using both temperature data and numerical simulations. An initial numerical experiment demonstrated that the internal mold state could be determined solely from the surface temperature values. A subsequent numerical experiment to validate this method showed that estimations based on surface temperatures were highly accurate in the case of degree of cure and internal temperature, although predictions of thermal conductivity were more difficult.

Keywords: Engineering, Materials science, Applied mathematics

https://doi.org/10.1016/j.heliyon.2018.e00554

1. Introduction

In order to produce high-quality carbon fiber-reinforced plastics (CFRP), CFRP molding state prediction via numerical simulations is considered an efficient method [1, 2, 3]. Predicting the CFRP molding state requires accurate modeling and understanding of the thermal behavior [4]. However, the molding state of CFRP varies over time and the model properties must change accordingly. Thus, modeling CFRP molding is extremely difficult. Owing to this reason, discrepancies normally appear between the CFRP molding state values predicted by numerical simulations and those of the actual molded products.

Therefore, instead of simply predicting the molding state with numerical simulations, "molding monitoring," which captures the molding state of the structure in real time, was conducted [5, 6, 7]. This process was conducted by investigating the molded product from the outside, by embedding sensors within the structure during production, and by installing sensors on the molding devices in order to monitor the cure reaction heat, distortion, temperature distribution, and percentage of voids in the resin during the molding process. However, the embedding of sensors in molded products led to a reduction in the quality of the molding. A molding optimization study with liquid composite molding (LCM) in which multiple artificial neural networks (ANNs) optimized the information signals obtained via wireless sensors used to monitor the molding processes was also performed [8]. However, ANNs require prior learning [9] and estimating entire states of complex structures from a small number of measured values is difficult.

Therefore, a study combining both numerical simulation and molding monitoring was performed. However, predicting the state of complex models is even more difficult. For example, consider the case of ply drop-off laminates used in the wing structures of airplanes [10, 11]; here, CFRP laminates are responsible for the distribution of heat in the cross-sectional direction and contains complex interior structures [12]. Heat molding with external heating causes irregular heat distributions, which generates molding defects such as warping, which is in turn caused by residual stress and curing distortion. In addition, because CFRP is a composite of carbon fiber and resin, its characteristic thermodynamics, molecular dynamics, and structural and performance parameters are uncertain; these factors further complicate accurate modeling.

By data assimilation, which integrates values forecasted by numerical simulation and values obtained by actual experiment and measurements, highly accurate state prediction and modeling can be achieved. Data assimilation is a state estimation method used in many fields, such as meteorology [13, 14, 15], hydrodynamics [16], soil science [17], and biomechanics [18]. Moreover, in the composite materials field, a method for analyzing resin impregnation behavior in resin transfer molding (RTM) has been proposed [19, 20, 21]. However, there is no literature available on

https://doi.org/10.1016/j.heliyon.2018.e00554

the heat transfer phenomena in the field of materials. Because molded composite materials are cured by heat, prediction of the heat transfer phenomena in molded products allows the prediction of the molding states of composite materials. However, heat transfer simulations are highly dependent on physical parameters; external factors and uncertainties create large discrepancies with actual heat transfer phenomena, thus limiting the accuracy of the predictions made using physical models. For this reason, with the application of data assimilation, which integrates simulated and experimental values, highly accurate state estimation and modeling may be expected even for CFRP laminates with complex internal structures.

Therefore, in this study, we propose a method to estimate the state of thermoset molding of CFRP using a data assimilation method that integrates estimated values from numerical simulations (as shown in Fig. 1) and experimentally measured values. This method estimates the distribution of temperature and degree of cure of a thermoset model in CFRP molding and its thermal conductivity distribution, which is a material property. The validity of the proposed method is also evaluated through numerical experiments.

2. Theory

2.1. CFRP thermosetting simulation

2.1.1. Non-stationary anisotropic heat transfer equation

To obtain the values forecasted by numerical simulation for data assimilation, a thermosetting simulation of CFRP is used. If the main axis directions are assumed as the *x*-*y* axes, the relationship between heat flux density and temperature during the process of heat transfer in an anisotropic material like CFRP follows Fourier's law as shown in Eqs. (1) and (2).

$$\mathbf{J} = -\mathbf{k}\,\mathrm{grad}\,T \tag{1}$$

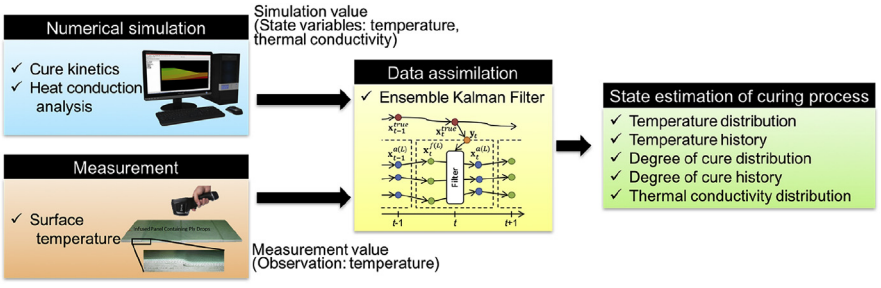

Fig. 1. Diagram of the state estimation method with data assimilation in CFRP thermosetting molding. The values forecasted by numerical simulation and experimentally measured values are integrated for state estimation.

https://doi.org/10.1016/j.heliyon.2018.e00554

$$\mathbf{k} = \begin{bmatrix} k_{xx} & 0 & 0 \\ 0 & k_{yy} & 0 \\ 0 & 0 & k_{zz} \end{bmatrix} \tag{2}$$

Here, **J** is the heat flux density and T is the absolute temperature. **k** is a thermal conductivity tensor, defined as shown in Eq. (2), where k_{xx}, k_{yy}, and k_{zz} indicate the thermal conductivities in each of the Cartesian coordinate directions.

The relationship with continuity, considering the internal generation of heat, is shown in Eq. (3).

$$\frac{\partial \rho_E}{\partial t} = -\mathrm{div}\,\mathbf{J} + \rho_r V_r \dot{Q} \tag{3}$$

Here, ρ_E is the energy density, ρ_r is the density of resin, V_r is the volume fraction of resin in the composite materials, and $\dot{Q}$ is the calorific value per unit of mass and time. The rate of change of energy density with respect to time is expressed by Eq. (4) in terms of the specific heat capacity and rate of change of temperature.

$$\frac{\partial \rho_E}{\partial t} = \rho c \frac{\partial T}{\partial t} \tag{4}$$

Here, ρ and c are the density and specific heat capacity, respectively, of the composite material.

Using Eqs. (1), (3), and (4), the equation for non-stationary anisotropic heat transfer can be written as Eq. (5).

$$\rho c \frac{\partial T}{\partial t} = \frac{\partial}{\partial x}\left(k_{xx}\frac{\partial T}{\partial x}\right) + \frac{\partial}{\partial y}\left(k_{yy}\frac{\partial T}{\partial y}\right) + \frac{\partial}{\partial z}\left(k_{zz}\frac{\partial T}{\partial z}\right) + \rho_r V_r \dot{Q} \tag{5}$$

2.1.2. Resin curing rule

Many thermosetting resins, such as epoxy resins, are used in CFRP. When heat is applied to a thermosetting resin, the matrix and curing agents undergo a chemical reaction and form a cross-linked structure through which the curing process progresses. In addition, curing reaction heat is generated from the resin itself as the cross-linked structure develops. The calorific value per unit time is expressed as Eq. (6).

$$\dot{Q} = \frac{dQ}{dt} = H_r \frac{d\alpha}{dt} \tag{6}$$

Here, α is the degree of cure and H_r is the total reaction heat.

The cure reactions of thermosetting resins are expressed as curing rules from the model equation proposed by Kamal and Sourour [22] and the Arrhenius equation [23] (Eqs. (7) and (8)).

https://doi.org/10.1016/j.heliyon.2018.e00554

$$\frac{d\alpha}{dt} = (K_1 + K_2\alpha^m)(1-\alpha)^n \tag{7}$$

$$K_i = A_i \exp\left(\frac{-\Delta E_i}{RT}\right) \quad (i = 1,2) \tag{8}$$

Here, m and n refer to the degree of reaction, K_i is the reaction speed constant, A_i is the frequency factor, ΔE_i is the activation energy, and R is the gas constant.

2.1.3. Formulation of the CFRP thermosetting simulation

When the finite element method is applied to solve the differential equation of non-stationary anisotropic heat transfer described in section 2.1.1, Eq. (9) is obtained [23,24,25].

$$\mathbf{K}\boldsymbol{\varphi} + \mathbf{C}\frac{\partial \boldsymbol{\varphi}}{\partial t} = \mathbf{f} \tag{9}$$

Here, $\mathbf{K}$ is the element of the heat transfer matrix, $\mathbf{C}$ is the element of the thermal capacity matrix, and $\mathbf{f}$ is the element of the heat flux vector; these parameters are defined as Eqs. (10), (11) and (12).

$$\mathbf{K} = \int_A \left(k_{xx}\frac{\partial\{N\}}{\partial x}\frac{\partial\{N\}^T}{\partial x} + k_{yy}\frac{\partial\{N\}}{\partial y}\frac{\partial\{N\}^T}{\partial y}\right)dA + \int_{A_3} h\{N\}\{N\}^T dA \tag{10}$$

$$\mathbf{C} = \int_A \rho c\{N\}\{N\}^T dA \tag{11}$$

$$\mathbf{f} = \int_A \rho_r V_r \dot{Q}\{N\}^T dA - \int_{A_2} q_0\{N\}dA + \int_{A_3} hT_{fluid}\{N\}dA \tag{12}$$

Because Eq. (9) contains a non-static term, a time difference term is applied by the Crank-Nicolson's implicit method [26], which produces Eq. (13).

$$\left(\frac{1}{2}\mathbf{K} + \frac{1}{\Delta t}\mathbf{C}\right)\boldsymbol{\varphi}_t = \left(-\frac{1}{2}\mathbf{K} + \frac{1}{\Delta t}\mathbf{C}\right)\boldsymbol{\varphi}_{t-1} + \frac{\mathbf{f}_t + \mathbf{f}_{t-1}}{2} \tag{13}$$

Here, Δt indicates time increment and the subscript t indicates time. Using Eq. (13), a thermosetting simulation, which takes into account internal heat generation, can be performed.

2.2. State estimation with data assimilation

2.2.1. Calculation algorithm of an ensemble Kalman filter

The thermosetting simulation performed in this study is a non-linear state space; therefore, we considered the ensemble Kalman filter (EnKF) as an effective tool

https://doi.org/10.1016/j.heliyon.2018.e00554

for state estimation by data assimilation as it supports non-linear models. EnKF estimates the true state by assimilating the observed values from measurements with respect to the forecasted values of multiple ensembles of time evolution. Fig. 1 shows the schematic diagram of the state estimation method with data assimilation in CFRP thermosetting molding. The integration of numerical simulation and experiments was performed using an ensemble Kalman filter. In this ensemble Kalman filter, the state variables of temperature and thermal conductivity were updated using

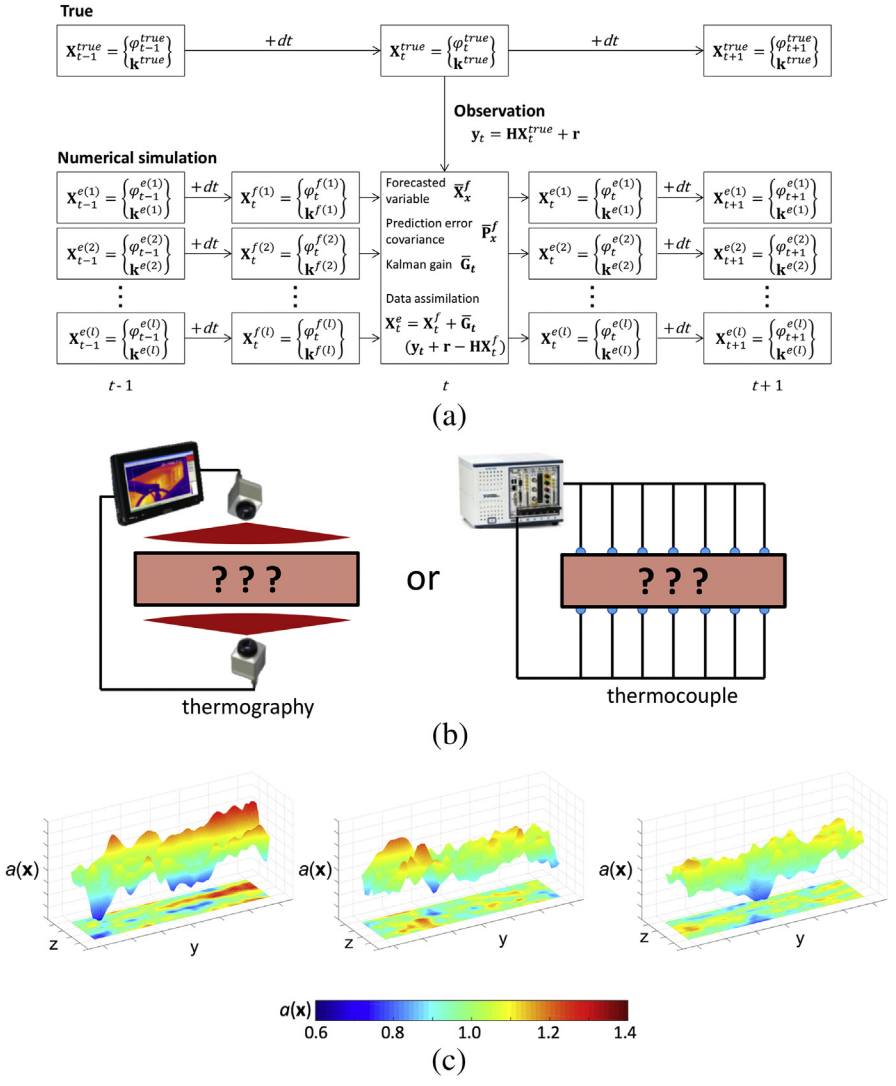

Fig. 2. Calculation flow and modeling for state estimation by data assimilation. (a) Calculation algorithm of EnKF. Multiple ensemble members are created and forecasted values are corrected through the creation of forecasted values and filtering operations. (b) Schematic of observation method for the model state. The surface temperature distributions at the top and bottom surfaces are measured. (c) Example of initial thermal conductivity distributions of ensembles generated from the KL expansion of parameter vector $\boldsymbol{\beta}_i$.

https://doi.org/10.1016/j.heliyon.2018.e00554

numerical simulation, and thereafter, the state variables were filtered by using the measured value of temperature. Fig. 2(a) shows the flow of the calculation of EnKF.

If the state vector at time t with respect to the non-linear model is defined as $\mathbf{x}_t$, the state transition of the numerical simulation system can be expressed by Eq. (14).

$$\mathbf{x}_t = \mathbf{F}_t(\mathbf{x}_{t-1}, \mathbf{w}_t) \tag{14}$$

where $\mathbf{F}_t$ is the time evolution operator, $\mathbf{w}_t$ represents system noise, and Eq. (14) is the system state equation. Furthermore, the observation equation that maps the state vector $\mathbf{x}_t$ to the observation value $\mathbf{y}_t$ can be written as Eq. (15).

$$\mathbf{y}_t = \mathbf{H}\mathbf{x}_t + \mathbf{r}_t \tag{15}$$

where $\mathbf{H}$ is an observation matrix that transfers the state vector to the observation value and $\mathbf{r}_t$ is an observation error vector.

The flow of state estimation algorithm with EnKF proceeds as follows:

(1) Initial values for multiple ensembles are created from the predicted distribution of the state vector $\mathbf{x}_t$ at time $t = 0$ (Eq. (16)).

$$\left\{\mathbf{x}_0^{\mathrm{e}(1)}, \mathbf{x}_0^{\mathrm{e}(2)}, \cdots, \mathbf{x}_0^{\mathrm{e}(L)}\right\} \tag{16}$$

The superscript e represents "estimation," while L is the number of ensemble members.

(2) Time elapses for each ensemble member according to Eq. (14) to obtain the ensemble forecasted value $\mathbf{x}_t^{\mathrm{f}(l)}$ at time t, one period ahead (Eq. (17)).

$$\mathbf{x}_t^{\mathrm{f}(l)} = \mathbf{F}_t\left(\mathbf{x}_{t-1}^{\mathrm{e}(l)}, \mathbf{w}_t^{\mathrm{e}(l)}\right) \tag{17}$$

The superscript f is the initial letter of "forecast." $\mathbf{x}_{t-1}^{\mathrm{e}(l)}$ and $\mathbf{w}_t^{\mathrm{e}(l)}$ is the state vector at time $t-1$ and the system noise at time t, respectively.

(3) From the ensemble forecasted value, $\mathbf{x}_t^{\mathrm{f}(l)}$, the average value $\overline{\mathbf{x}}_t^{\mathrm{f}}$, covariance matrix for prediction error $\overline{\mathbf{P}}_t^{\mathrm{f}}$, and Kalman gain $\overline{\mathbf{G}}_t$ are calculated according to Eqs. (18), (19), and (20).

$$\overline{\mathbf{x}}_t^{\mathrm{f}} = \frac{1}{L}\sum_{l=1}^{L}\mathbf{x}_t^{\mathrm{f}(l)} \tag{18}$$

$$\overline{\mathbf{P}}_t^{\mathrm{f}} = \frac{1}{L-1}\sum_{l=1}^{L}\left(\mathbf{x}_t^{\mathrm{f}(l)} - \overline{\mathbf{x}}_t^{\mathrm{f}}\right)\left(\mathbf{x}_t^{\mathrm{f}(l)} - \overline{\mathbf{x}}_t^{\mathrm{f}}\right)^{\mathrm{T}} \tag{19}$$

$$\overline{\mathbf{G}}_t = \overline{\mathbf{P}}_t^{\mathrm{f}}\mathbf{H}^{\mathrm{T}}\left(\mathbf{H}\overline{\mathbf{P}}_t^{\mathrm{f}}\mathbf{H}^{\mathrm{T}} + \mathbf{R}\right)^{-1} \tag{20}$$

$\mathbf{R}$ is the covariance matrix corresponding to the observation error.

https://doi.org/10.1016/j.heliyon.2018.e00554

(4) The observation value $\mathbf{y}_t$ is assimilated into the forecasted value $\mathbf{x}_t^{\mathrm{f}(l)}$ using Eq. (21), which uses Kalman gain $\overline{\mathbf{G}}_t$ to calculate the ensemble estimated value $\mathbf{x}_t^{\mathrm{e}(l)}$.

$$\mathbf{x}_t^{\mathrm{e}(l)} = \mathbf{x}_t^{\mathrm{f}(l)} + \overline{\mathbf{G}}_t\left(\mathbf{y}_t + \mathbf{r}_t^{(l)} - \mathbf{H}\mathbf{x}_t^{\mathrm{f}(l)}\right) \tag{21}$$

$\mathbf{y}_t + \mathbf{r}_t{}^{(l)}$ is referred to as the perturbed observation and ensemble approximation when the linear Gaussian state space matches the Kalman gain produced by the Kalman filter.

(5) The average value $\overline{\mathbf{x}}_t^{\mathrm{e}}$ is calculated from the ensemble estimated value $\mathbf{x}_t^{\mathrm{e}(l)}$ and defined as the estimated value at time t (Eq. (22)).

$$\overline{\mathbf{x}}_t^{\mathrm{e}} = \frac{1}{L}\sum_{l=1}^{L}\mathbf{x}_t^{\mathrm{e}(l)} \tag{22}$$

(6) Steps (1) to (5) are repeated until the analysis is concluded.

2.2.2. Model observation method

In order to measure the internal state of a product during the thermoset molding of CFRP, it is necessary to embed a sensor in the molded product in advance. However, embedding sensors may degrade the quality of the molded product. Therefore, it is assumed that the model surface temperature is measured using thermography and a thermocouple. This study assumes the measurement of the temperature distribution of a continuous model surface as shown in Fig. 2(b). Eq. (23) is the observation value $\mathbf{y}_t$ obtained by measurement.

$$\mathbf{y}_t = \begin{Bmatrix} T_t^1 \\ T_t^2 \\ \vdots \\ T_t^i \end{Bmatrix} \tag{23}$$

T_t is the observation temperature and the superscript i represents the measurement location.

2.2.3. Ensemble initial value generation with Karhunen-Loève expansion

The thermal conductivity of CFRP is spatially non-uniform, varying according to the resin combination ratio, resin distribution in the molded product, and the orientation of the carbon fiber [4]; therefore, it is difficult to determine the thermal conductivity distribution accurately prior to simulation. In order to logically predict the temperature distribution, it is necessary to treat the thermal conductivity distribution assuming that it includes a certain degree of uncertainty; further, it is also necessary to conduct a stochastic heat transfer simulation.

https://doi.org/10.1016/j.heliyon.2018.e00554

Because the thermal conductivity tensor **k** is a second-order symmetric tensor, it is necessary to design and estimate a probability model to model the uncertainty with high accuracy. However, the main objective of this study is to estimate thermal conductivity distribution via data assimilation of observed and forecasted values; we do not detail the statistical modeling of the thermal conductivity distribution. Instead, we focus on formulating the generation of the initial value for thermal conductivity using the Karhunen-Loève (KL) expansion with the objective of representing the thermal conductivity distribution, which is a model parameter of various ensembles in EnKF.

Considering the thermal conductivity as a property that changes positionally, it can be represented using the stochastic process $a(\mathbf{x})$ as Eq. (24).

$$\mathbf{k}(\mathbf{x}) = \overline{\mathbf{k}}\, a(\mathbf{x}) \tag{24}$$

Here, $\mathbf{x}$ is the position vector, $\overline{\mathbf{k}}$ is the average thermal conductivity tensor, and $a(\mathbf{x})$ is a stochastic process defined as average $E[a(\mathbf{x})] = 1$. The covariance function, $\mathrm{cov}(a(\mathbf{x}), a(\mathbf{x}'))$, can be expressed using Eq. (25).

$$\mathrm{cov}(a(\mathbf{x}),\, a(\mathbf{x}')) = \sigma_a^2 \exp\left[-\frac{|x-x'|}{\eta_x} - \frac{|y-y'|}{\eta_y} - \frac{|z-z'|}{\eta_z} \right] \tag{25}$$

Here, σ_a^2 is the variation of α and η_x, η_y, and η_z are the correlation lengths of each of the coordinate components. Eq. (25) indicates that the covariance αat two points becomes higher as the distance between the two points decreases. By using this equation, α can be sampled independent of the mesh size of FEM. Because the stochastic process $a(\mathbf{x})$ in this formulation can assume many values, it can represent not only those thermal conductivity distributions that may occur in an actual experiment, but also those that are extremely unlikely to occur. At this point, it is possible to apply spectral decomposition to the covariance function as Eq. (26).

$$\mathrm{cov}(a(\mathbf{x}), a(\mathbf{x}')) = \sum_{i=1}^{\infty} \lambda_i \phi_i(\mathbf{x}) \phi_i(\mathbf{x}') \tag{26}$$

λ_i and $\phi_i(\mathbf{x})$ represent the eigenvalue and eigenfunction of the covariance function, respectively. If KL expansion is used to retain the eigenvalues of the stochastic process $a(\mathbf{x})$ up to the maximum number Q and truncate those below it, it can be expanded as Eq. (27).

$$a(\mathbf{x}) \approx a_Q(\mathbf{x}) = 1 + \sum_{i=1}^{Q} \sqrt{\lambda_i}\, \phi_i(\mathbf{x}) \beta_i \tag{27}$$

Here, $\beta_i = \{\beta_1, \cdots, \beta_i, \cdots\}$ is a parameter vector with probability variables as components. These probabilities follow a mutually independent standard normal distribution (normal distribution with average 0 and variance 1). With this approximation, it is possible to use parameter vectors with independent probability variables as components to represent a variety of thermal conductivity distributions. The thermal conductivity

https://doi.org/10.1016/j.heliyon.2018.e00554

distribution generated here is used as the initial thermal conductivity of the ensemble in EnKF. Fig. 2 (c) shows an example of the ensemble initial value with KL expansion.

2.2.4. Formulation of state estimation method with EnKF

The state estimation with EnKF is formulated through a combination of the thermosetting simulation shown in section 2.1, the EnKF algorithm shown in section 2.2.1, the model observation method shown in section 2.2.2, and the ensemble initial value generation with KL expansion shown in section 2.2.3. In the CFRP thermosetting simulation, the state vector $\mathbf{x}_t$ of the model is defined by the nodal temperature vector $\boldsymbol{\varphi}_t$, which represents the temperature distribution, and the parameter vector $\boldsymbol{\beta}_t$, which represents the thermal conductivity distribution as shown in Eq. (28).

$$\mathbf{x}_t = \begin{Bmatrix} \boldsymbol{\varphi}_t \\ \boldsymbol{\beta}_t \end{Bmatrix} \tag{28}$$

Using the above equation, it is possible to estimate not only the nodal temperature vector $\boldsymbol{\varphi}_t$, which indicates the model state, but also the thermal conductivity distribution, which is a model parameter. The system equation at time t follows the equation shown in Eq. (29).

$$\mathbf{x}_t = \left(\frac{1}{2}\mathbf{K} + \frac{1}{\Delta t}\mathbf{C}\right)^{-1}\left(-\frac{1}{2}\mathbf{K} + \frac{1}{\Delta t}\mathbf{C}\right)\mathbf{x}_{t-1} + \left(\frac{1}{2}\mathbf{K} + \frac{1}{\Delta t}\mathbf{C}\right)^{-1}\left(\frac{\mathbf{f}_t + \mathbf{f}_{t-1}}{2}\right) \tag{29}$$

Eq. (30) is the observation equation which correlates the observation value $\mathbf{y}_t$ from Eq. (15) and the state vector $\mathbf{x}_t$ from Eq. (28).

$$\mathbf{y}_t = [\mathbf{H} \quad 0]\begin{Bmatrix} \boldsymbol{\varphi}_t \\ \boldsymbol{\beta}_t \end{Bmatrix} = \overline{\mathbf{H}}\mathbf{x}_t + \mathbf{r}_t \tag{30}$$

In addition, when the parameter vector $\boldsymbol{\beta}_t$, which uses random numbers following a standard normal distribution, is expressed with KL expansion, the initial value of the ensemble member is generated (Eq. (31)).

$$\left\{\mathbf{x}_0^{\mathrm{e}(1)}, \mathbf{x}_0^{\mathrm{e}(2)}, \cdots, \mathbf{x}_0^{\mathrm{e}(L)}\right\} \tag{31}$$

With the state vector, system state equation, observation equation, and ensemble member initial value described above, steps (1) to (5) listed in section 2.2.1 are repeated to estimate the model state.

If the parameter vector $\boldsymbol{\beta}_t$ changes drastically, the numerical calculation becomes unstable. For this reason, we adopt a practical method using the smoothing parameter γ to stabilize changes in the parameter vector as shown in Eq. (32) [27].

https://doi.org/10.1016/j.heliyon.2018.e00554

$$\boldsymbol{\beta}_t^{f(l)} = \gamma\,\boldsymbol{\beta}_{t-1}^{f(l)} + (1-\gamma)\boldsymbol{\beta}_{t-1}^{a(l)} \tag{32}$$

Here, $\boldsymbol{\beta}_{t-1}^{f(l)}$ and $\boldsymbol{\beta}_{t-1}^{a(l)}$ are the predicted and estimated values of the parameter vector of ensemble member l at time $t-1$.

3. Model

3.1. Problem definition

The validity of the proposed state estimation method with EnKF is evaluated. In actual applications, experimentally measured values are used as the observed values for data assimilation; however, to evaluate the estimation accuracy, the experiment here is simulated via numerical methods. A thermosetting simulation is performed with an arbitrarily defined thermal conductivity distribution and the analysis values for temperature and degree of cure are defined as the true values of the model. The temperature distribution of the model surface is observed via the method shown in section 2.2.2. At the moment of measurement, a random number following a normal distribution is added as the observation error.

We conducted a state estimation with EnKF, which uses model observation values to evaluate the validity of the proposed method by comparing the estimated model state

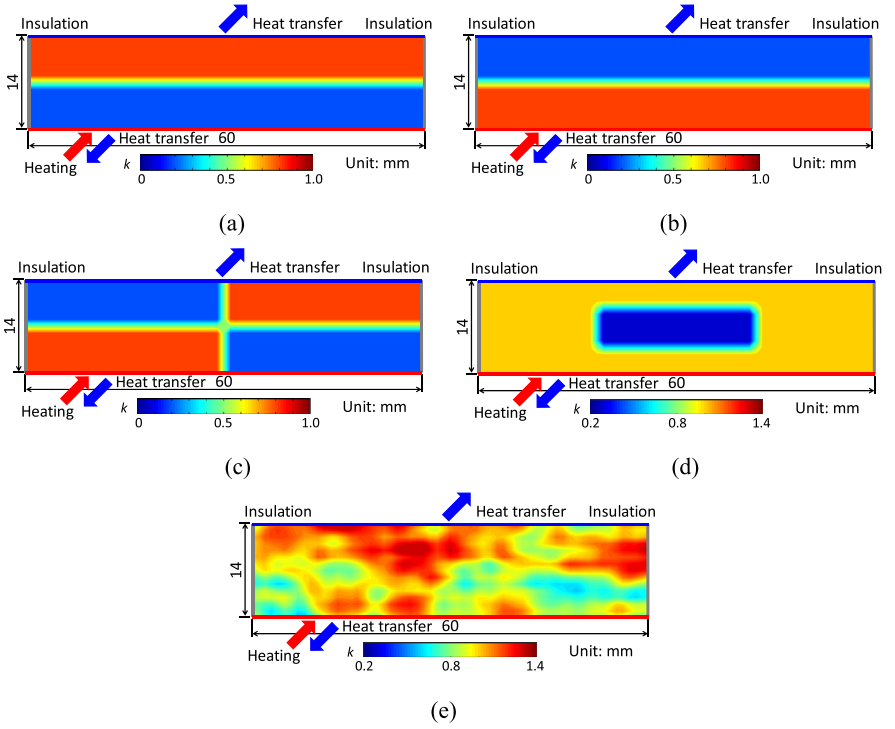

Fig. 3. True values and analysis conditions for the thermal conductivity distribution of the evaluation model. (a) High-k top, low-k bottom, (b) low-k top, high-k bottom, (c) cross-sectional split, (d) central low-k, and (e) inhomogeneous k distribution.

https://doi.org/10.1016/j.heliyon.2018.e00554

(defined by the temperature and degree of cure) and the model parameter of thermal conductivity distribution against the true values. As an evaluation model, a multiple-ensemble model with varied thermal conductivity distributions, as shown in Fig. 3, is prepared. First, we change the observation method according to the model shown in Fig. 3(d) and estimate the temperature, degree of cure, and thermal conductivity to evaluate the influence of the observation method on the accuracy of the estimation. Next, we estimate the state of temperature, degree of cure, and thermal conductivity with respect to the thermal conductivity distribution models shown in Fig. 3 and evaluate the influence of thermal conductivity distribution on the estimated values.

A two-dimensional model that simulates CFRP laminates is used for evaluation. The geometry of the model was rectangular with the dimensions of 14 mm × 60 mm. The FE mesh was created with the dimensions of 1 mm × 1 mm for each node; therefore, there were 915 nodes and 840 elements in total. The coordinate system of the model yields the thermal property values of CFRP shown in Table 1, with the x-axis (normal to the page) following the 0° direction, the y-axis following the 90° direction, and the z axis following the out-of-plane direction. The values in Table 2 are used as curing rule parameters for the epoxy resin. The model is heated uniformly from the lower side and the analysis conditions are defined as heat transfer from the upper part of the model to the surrounding atmosphere during curing, as well as heat transfer from the lower part of the model to the heated part. The parameters used in the analysis are shown in Table 3. Although uniform heating is assumed in this study, data assimilation can be applied to non-uniform heating by modifying the heating pattern in the numerical simulation.

3.2. Evaluation index of estimation accuracy

As evaluation indices of state estimation accuracy, we used the root mean square error (RMSE) normalized by the number of nodes at time t and the time mean error (TME) of RMSE as shown in Eqs. (33) and (34), respectively. As RMSE depicts the error of the true value, it cannot quantitatively compare the distribution tendencies of the true versus estimated values. Therefore, the distribution tendency is evaluated using Pearson's moment correlation coefficient as shown in Eq. (35).

Table 1. Thermal properties of epoxy resin, carbon fiber (T800S), and CFRP (V_f = 0.57, 20 °C).

Materials	Density $\rho_{r,\,c,\,cfrp}$ [kg/m^3]	Specific heat $c_{r,\,c,\,cfrp}$ [J/kg·°C]	Thermal conductivity $k_{xx,\,yy,\,zz}$ [W/m·°C]
Epoxy resin	1200	1600	0.20
Carbon fiber (T800S)	1800	760	10.0
CFRP (V_f = 0.57, 20 °C)	1540	1040	k_{xx} (0°) = 9.0 k_{yy} (90°) = 0.77 k_{zz} (transverse) = 0.70

https://doi.org/10.1016/j.heliyon.2018.e00554

Table 2. Cure kinetics parameters of epoxy resin.

Description	Parameter	Value
Total heat of reaction	H_r [J/kg]	4.63×10^5
Pre-exponential coefficient	A_1 [1/s]	42.9
	A_2 [1/s]	3.97×10^5
Activation energy	ΔE_1 [J/mol]	4.37×10^4
	ΔE_2 [J/mol]	6.99×10^4
Reaction order	m	1.08
	n	2.66
Universal gas constant	R [J/(mol·°C)]	8.3145

Table 3. Parameters used for the numerical analysis of data assimilation using EnKF.

Description	Parameter	Value
Number of elements	Ne [-]	840
Number of nodes	Np [-]	915
Analysis time	t [s]	7200
Numerical simulation interval	Δt [s]	1.0
Initial (ambient) temperature	$T_0 = T_{air}$ [°C]	25
Heat transfer coefficient	h_{air} [W/m^2·°C]	5.0
	h_{heat} [W/m^2·°C]	50
Rate of temperature rise	T_{heat} [°C/min] (up to 180 °C)	5.0
Data assimilation time interval	Δt_{DA} [s]	Δt
Correlation length	η_x [m]	0.0060
	η_y [m]	0.0014
Dimension of parameter vector $\boldsymbol{\beta}$	Q [-]	Fig. 3(a)–(c) 200 Fig. 3(d), (e) 300
Number of ensemble members	L [-]	Fig. 3(a)–(c) 25 Fig. 3(d), (e) 50
Smoothing coefficient	γ [-]	0.8

$$RMSE_t = \sqrt{\frac{1}{N}\sum_{i=1}^{N}\left(x^a_{i(t)} - x^{true}_{i(t)}\right)^2} \tag{33}$$

$$TME = \frac{1}{T}\sum_{i=1}^{T} RMSE_i \tag{34}$$

$$Correlation\ Coefficient = \frac{\sum_{i=1}^{N}\left(x^a_{i(t)} - \overline{x^a_{i(t)}}\right)\left(x^{true}_{i(t)} - \overline{x^{true}_{i(t)}}\right)}{\sqrt{\sum_{i=1}^{N}\left(x^a_{i(t)} - \overline{x^a_{i(t)}}\right)^2}\sqrt{\sum_{i=1}^{N}\left(x^{true}_{i(t)} - \overline{x^{true}_{i(t)}}\right)^2}} \tag{35}$$

https://doi.org/10.1016/j.heliyon.2018.e00554

N is the number of nodes, $x^{a}_{i(t)}$ is the estimated value of node i at time t, $x^{true}_{i(t)}$ is the true value of node i at time t, T is the number of time steps at the end of the analysis, $\overline{x^{a}_{(t)}}$ is the average estimated value at time t, and $\overline{x^{true}_{(t)}}$ is the average true value at time t.

4. Results and discussion

4.1. Effect of the number of observations

To evaluate the influence of the number of observations, we conducted an analysis with the same model (Fig. 3 (d)), changing only the number of observations. In "Full observation," 915 observations were made with all the nodes of the model as the observation values; in the "Top/middle/bottom observation," 183 observations were made with the top, middle, and bottom layers of the model as observation values; in the "Top/bottom observation," 122 observations were made with the top and bottom layers of the model as the observation values (Fig. 4 (a)).

Fig. 4(b) shows the representative time history of the measured and estimated temperature and the degree of cure for the central low k model with top/bottom observation. Highly accurate estimation was possible at the top and bottom of the model, whereas some estimation error occurred at the middle. RMSE (Eq. (33)) evaluation in Fig. 4 (c) and (d) indicates that the error fluctuates in a heated state, but throughout the analysis time, larger numbers of observations correspond to higher estimation accuracies. The evaluation of TME (Eq. (34)) in Fig. 4 (e) and (f) also indicates that a larger number of observations yields a more accurate estimation. Therefore, it is possible to say that in the state estimation with the proposed data assimilation method, the number of observations strongly influences the estimation performance. However, when estimating the internal state of the model from the surface temperature information, similar to the observation model using the top and bottom layers, estimation accuracy is low compared to the observations using the entire model but the temperature is highly accurate, with a time-averaged error of approximately 1 °C.

In addition, as shown in Fig. 5 (a) to (c), when the true and final estimation values of the thermal conductivity distribution are evaluated, a low thermal conductivity distribution is estimated in the middle layer not only in the "Full observation" and "Top/middle/bottom" models, but also in the "Top/bottom" observation model. As Fig. 5 (d) shows, when the correlation coefficient with the true value is evaluated quantitatively, larger numbers of observations correspond to higher correlation coefficient values. In the case of the "Top/bottom observation," a qualitative evaluation suggests that a low thermal conductivity distribution can be estimated; with a quantitative correlation coefficient, a moderate positive correlation of 0.354 is indicated.

https://doi.org/10.1016/j.heliyon.2018.e00554

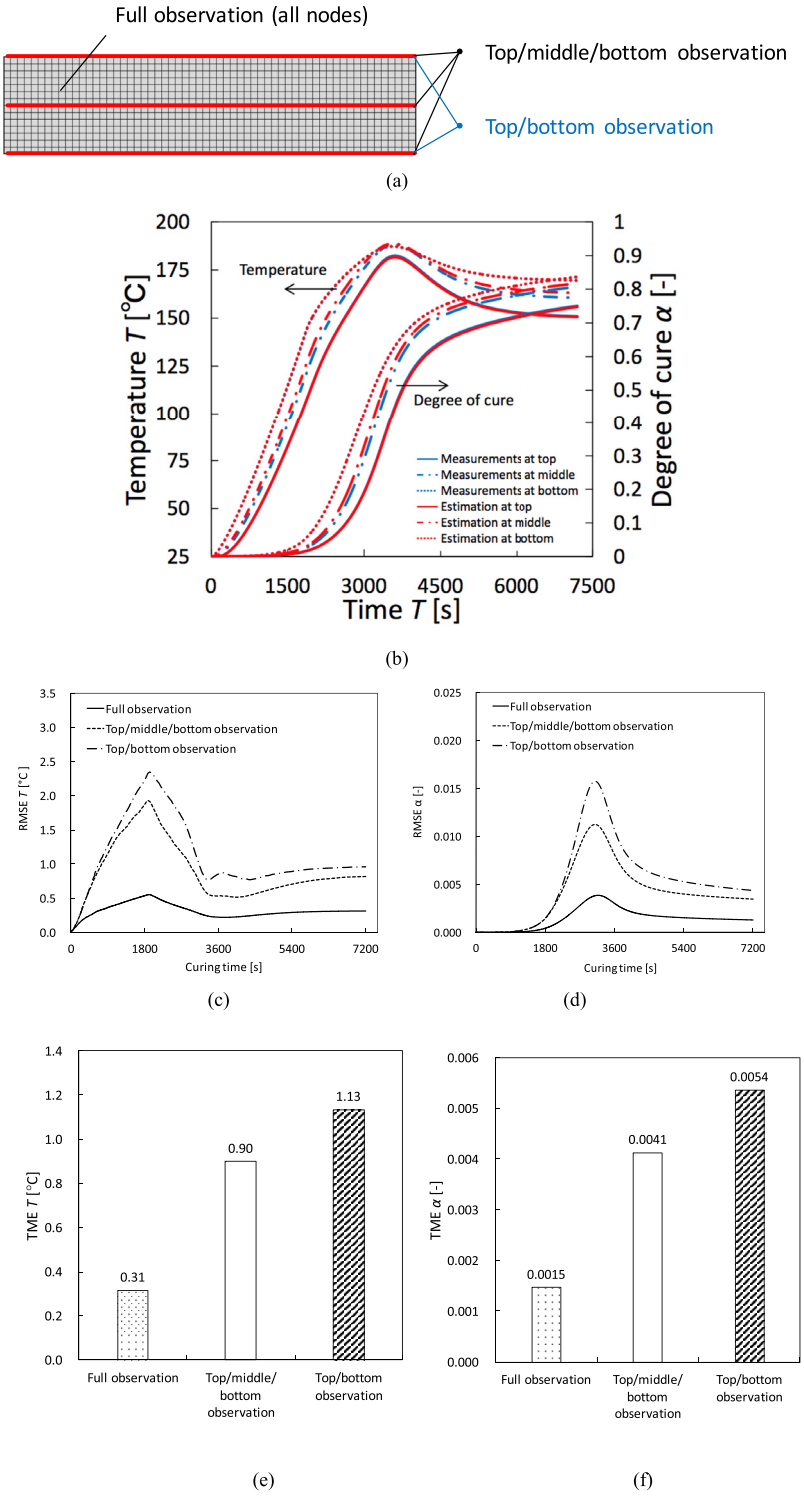

Fig. 4. Results of the estimation accuracy of the model state (temperature T and degree of cure α) using different observation methods. (a) Finite element mesh with various observation methods (b) Measured and estimated temperature and degree of cure for the central low k model with top/bottom observation (c) RMSE (root mean square error) T, (d) RMSE α, (e) TME (time mean error) T, and (f) TME α.

https://doi.org/10.1016/j.heliyon.2018.e00554

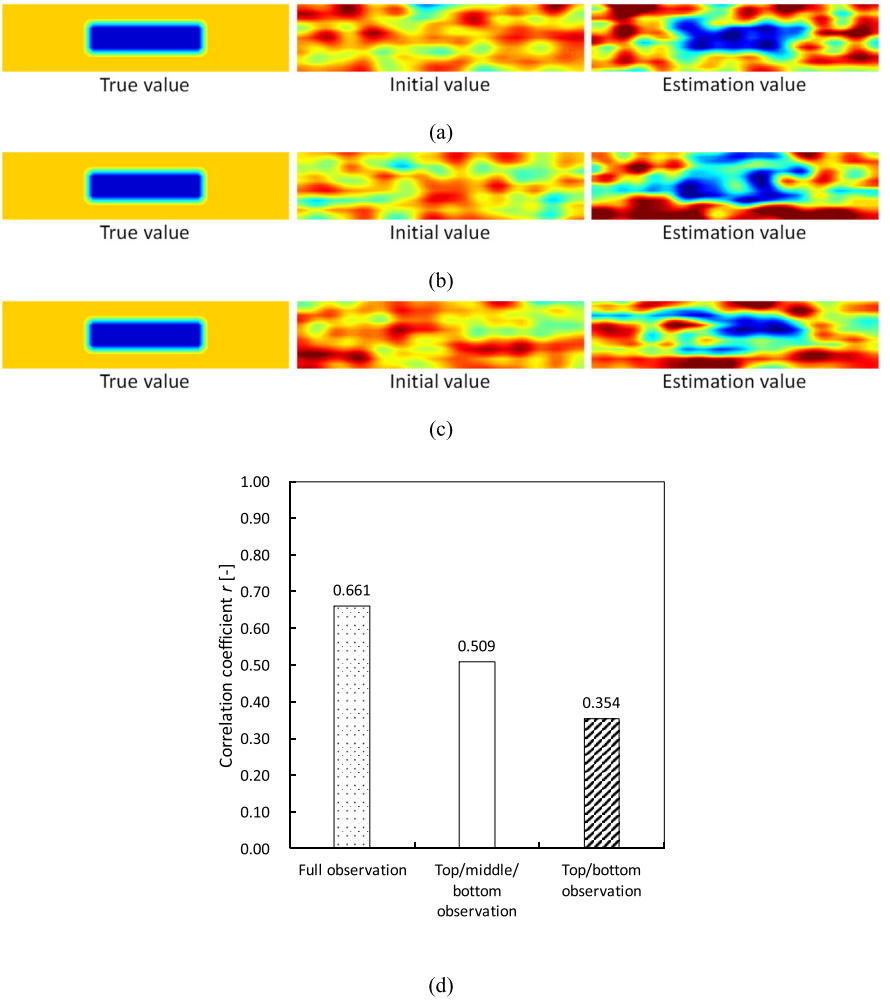

Fig. 5. Thermal conductivity distributions estimated using different observation methods. (a) Full observation model. (b) Top/middle/bottom observation model. (c) Top/bottom observation model (the left panel indicates the true value, the center panel corresponds to the estimation initial value, and the right panel depicts the final estimated value). (d) Correlation coefficient r of the true and estimated thermal conductivities.

The above findings demonstrate that with the state estimation method using data assimilation, more internal observation information contributes to a higher estimation accuracy. We also conclude that it is possible to estimate model parameters, such as the thermal conductivity distribution, internal temperature, and degree of cure of the model from partial observations of the model surface.

4.2. Effect of the thermal conductivity distribution

In order to evaluate the influence of the thermal conductivity distribution generated by the evaluation model, we conducted an analysis with the same conditions as the model with various distribution behaviors as shown in Fig. 3.

https://doi.org/10.1016/j.heliyon.2018.e00554

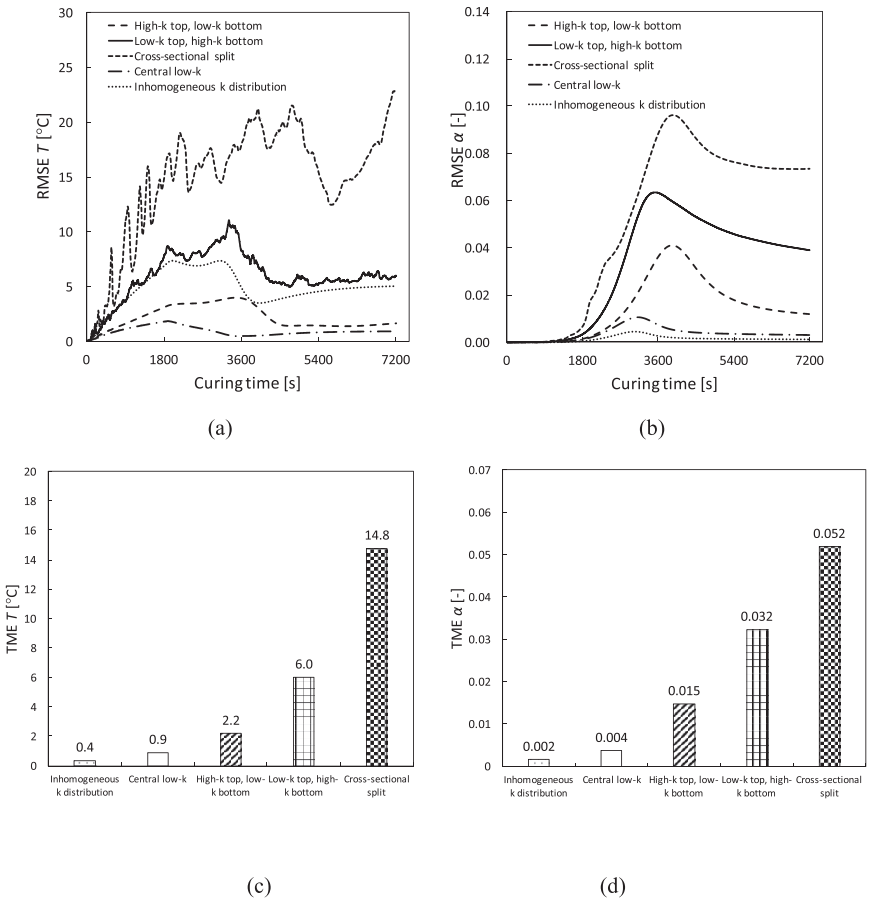

Fig. 6. Results of the estimation accuracy of the model state (temperature T and degree of cure α) evaluated using various thermal conductivity distribution models. (a) RMSE (root mean square error) T, (b) RMSE α, (c) TME (time mean error) T, and (d) TME α.

In evaluating the temperature and degree of cure, which are model states, with the RMSE shown in Fig. 6 (a) and (b) for all models, the estimation error increases when the temperature increases, but either decreases or stabilizes in the steady state. Fig. 6 (c) and (d) show the TME value of the model state. Compared to the models with a central low-*k* and inhomogeneous *k* distributions, the model with the thermal conductivity divided into top and bottom portions (i.e. high-*k* top, low-*k* bottom; low-*k* top, high-*k* bottom; cross-sectional split) has a low estimation accuracy. Because the evaluation model is heated from the bottom to the top, in the models without thermal conductivity distributions orthogonal to the direction of heat transfer, the temperature distributions in the top and bottom layers of the model are roughly uniform. In order to estimate the thermal conductivity distribution in the heat-transfer direction, it is necessary to rely on the difference between the heat transfer speeds of the true and estimated values and the decreased accuracy is attributed to insufficient amount of information.

Reviewing the estimated values of the thermal conductivity distribution shown in Fig. 7 (a) to (e), it is possible to see that a distribution tendency qualitatively similar

https://doi.org/10.1016/j.heliyon.2018.e00554

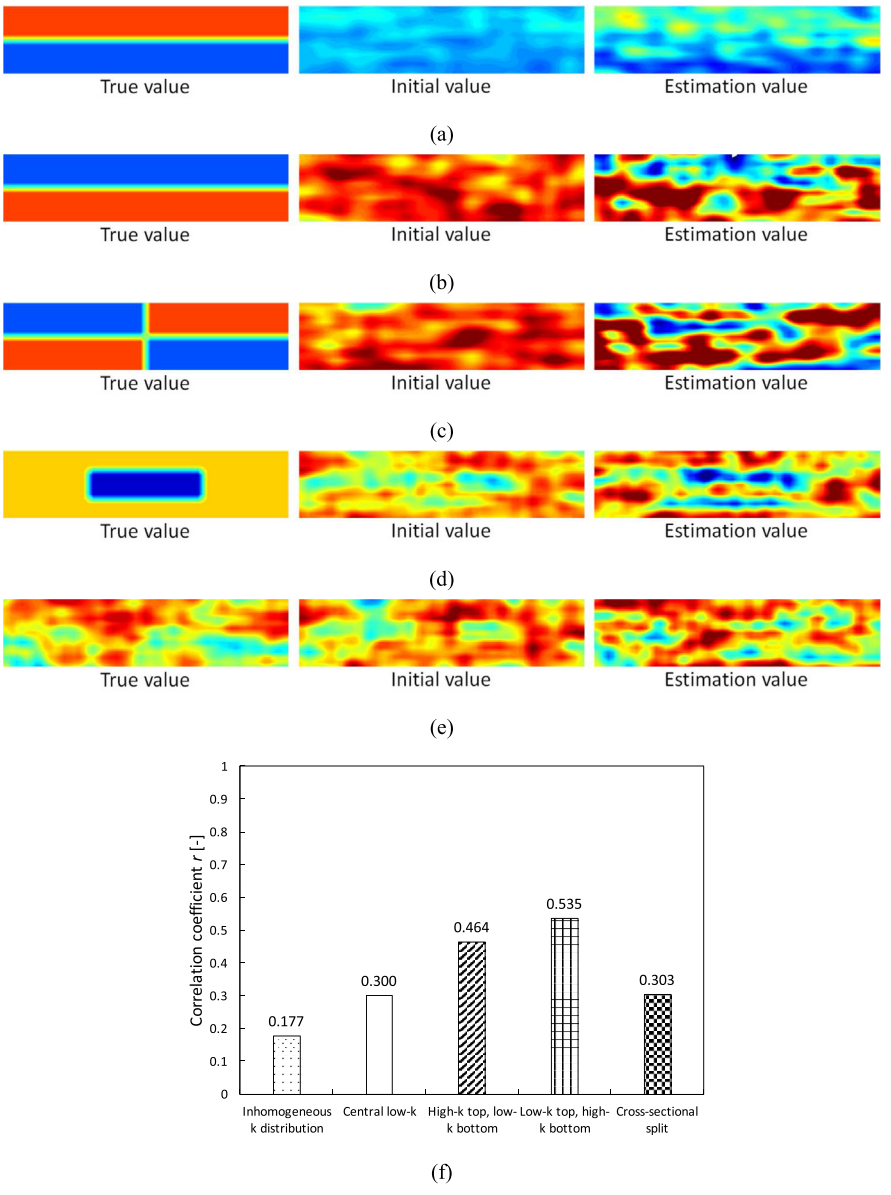

Fig. 7. Results of thermal conductivity distribution evaluated using various thermal conductivity distribution models: (a) high-k top, low-k bottom, (b) low-k top, high-k bottom, (c) cross-sectional split, (d) central low-k, and (e) inhomogeneous k distribution. (f) Correlation coefficient r of true and estimated thermal conductivities.

to that of the true value is obtained. From the correlation coefficient shown in Fig. 7 (f) as a quantitative evaluation of the distribution tendency, in the case of a relatively simple shape, an especially high correlation coefficient is obtained. However, in models with complex distributions, the correlation coefficient values are low. This is probably because the resolution of the estimation of thermal conductivity distribution is not high and therefore the method cannot provide localized estimations.

https://doi.org/10.1016/j.heliyon.2018.e00554

The above described results show that using the proposed method with observed values from the surface enabled the estimation of the internal states of models that are typically difficult to predict. It is also possible to estimate the tendency of the thermal conductivity distribution, which is a model parameter. However, it is clear that complex thermal conductivity distributions of the model cause difficulty in obtaining estimations that capture localized changes. To estimate thermal conductivity distributions with higher accuracy, it may be necessary to introduce more sophisticated methods of heating and observing the internal temperature state of the model.

5. Conclusion

In this study, we used data assimilation to unite a CFRP thermosetting simulation and surface temperature measurements to develop a method for estimating the thermoset state and material property values of CFRP; further, we evaluated the validity of the method. Initially, we conducted a numerical experiment to examine the influence of the observation method on the estimation accuracy of the internal temperature, degree of cure, and thermal conductivity. The results indicated that as the number of internal observation readings increased, the estimation accuracy of the state variables and model parameters improved; it was also possible to estimate the internal state using surface temperature alone. Furthermore, we created a model to define various thermal conductivity distributions and estimated the internal temperature, degree of cure, and thermal conductivity from the observed surface temperature values. The accuracy of the estimation was evaluated through a numerical experiment. The results indicated that even in cases with different thermal conductivity distributions, the data assimilation method enabled the estimation of the state of a model by integrating some of its observation values into the simulation. As an auxiliary function, the method also successfully estimated the distribution tendencies of the model parameters. In particular, for thermal conductivity distributions in which the temperature distribution of surfaces can be changed easily, the estimation of temperature and degree of cure were highly accurate. However, obtaining localized estimations of thermal conductivity in complex distributions was found to be a difficult task.

Declarations

Author contribution statement

R. Matsuzaki: Conceived and designed the experiments; Analyzed and interpreted the data; Wrote the paper.

T. Tachikawa: Conceived and designed the experiments; Performed the experiments; Analyzed and interpreted the data; Contributed reagents, materials, analysis tools or data; Wrote the paper.

https://doi.org/10.1016/j.heliyon.2018.e00554

J. Ishizuka: Analyzed and interpreted the data.

Funding statement

This work was supported by the Cross-ministerial Strategic Innovation Promotion Program (SIP), the "Innovative Structural Material Project" (Funding agency: JST).

Competing interest statement

The authors declare no conflict of interest.

Additional information

No additional information is available for this paper.

References

[1] S. Yi, H.H. Hilton, M.F. Ahmad, A finite element approach for cure simulation of thermosetting matrix composites, Comput. Struct. 64 (1) (1997) 383−388.

[2] S.C. Joshi, X.L. Liu, Y.C. Lam, A numerical approach to the modeling of polymer curing in fibre-reinforced composites, Compos. Sci. Technol. 59 (7) (1999) 1003−1013.

[3] T. Behzad, M. Sain, Finite element modeling of polymer curing in natural fiber reinforced composites, Compos. Sci. Technol. 67 (7-8) (2007) 1666−1673.

[4] M. Villière, D. Lecointe, V. Sobotka, N. Boyard, D. Delaunay, Experimental determination and modeling of thermal conductivity tensor of carbon/epoxy composite, Compos. Part A Appl. Sci. Manuf. 46 (2013) 60−68.

[5] G.M. Maistros, I.K. Partridge, Monitoring autoclave cure in commercial carbon fibre/epoxy composites, Compos. Part B Eng. 29 (3) (1998) 245−250.

[6] H.-K. Kang, D.-H. Kang, H.-J. Bang, C.-S. Hong, C.-G. Kim, Cure monitoring of composite laminates using fiber optic sensors, Smart Mater. Struct. 11 (2) (2002) 279.

[7] S. Konstantopoulos, E. Fauster, R. Schledjewski, Monitoring the production of FRP composites: a review of in-line sensing methods, Express Polym. Lett. 8 (11) (2014) 823−840.

[8] J. Zhang, N.G. Pantelelis, Modelling and optimisation control of polymer composite moulding processes using bootstrap aggregated neural network

https://doi.org/10.1016/j.heliyon.2018.e00554

models, in: Proceedings of 2011 International Conference on Electric Information and Control Engineering (ICEICE), 2011, pp. 2363–2366.

[9] Z. Zhang, K. Friedrich, Artificial neural networks applied to polymer composites: a review, Compos. Sci. Technol. 63 (14) (2003) 2029–2044.

[10] P. Dhurvey, N. Mittal, Review on various studies of composite laminates with ply drop-off, J. Eng. Appl. Sci. 8 (8) (2013) 595–605.

[11] K. He, S.V. Hoa, R. Ganesan, The study of tapered laminated composite structures: a review, Compos. Sci. Technol. 60 (14) (2000) 2643–2657.

[12] M. Mulle, F. Collombet, P. Olivier, R. Zitoune, C. Huchette, F. Laurin, Y.-H. Grunevald, Assessment of cure-residual strains through the thickness of carbon–epoxy laminates using FBGs Part II: technological specimen, Compos. Part A Appl. Sci. Manuf. 40 (10) (2009) 1534–1544.

[13] G. Burgers, P. Jan van Leeuwen, G. Evensen, Analysis scheme in the ensemble Kalman filter, Mon. Weather Rev. 126 (6) (1998) 1719–1724.

[14] J.L. Anderson, An ensemble adjustment Kalman filter for data assimilation, Mon. Weather Rev. 129 (12) (2001) 2884–2903.

[15] I.M. Navon, Data assimilation for numerical weather prediction: a review, in: S.K. Park, L. Xu (Eds.), Data Assimilation for Atmospheric, Oceanic and Hydrologic Applications, Springer, 2009, pp. 21–65.

[16] H. Kato, S. Obayashi, Approach for uncertainty of turbulence modeling based on data assimilation technique, Comp. Fluids 85 (2013) 2–7.

[17] B.X. Hu, J. Tong, Data assimilation application to the subsurface flow and solute transport, in: Hydraulic Conductivity, InTech, 2013.

[18] L. Wang, H. Zhang, K.C. Wong, H. Liu, P. Shi, Physiological-model-constrained noninvasive reconstruction of volumetric myocardial transmembrane potentials, IEEE Transact. Biomed. Eng. 57 (2) (2010) 296–315.

[19] M. Murata, R. Matsuzaki, A. Todoroki, Y. Mizutani, Y. Suzuki, Three-dimensional reconstruction of resin flow using capacitance sensor data assimilation during a liquid composite molding process: a numerical study, Compos. Part A Appl. Sci. Manuf. 73 (2015) 1–10.

[20] R. Matsuzaki, M. Shiota, Data assimilation through integration of stochastic resin flow simulation with visual observation during vacuum-assisted resin transfer molding: a numerical study, Compos. Part A Appl. Sci. Manuf. 84 (2016) 43–52.

https://doi.org/10.1016/j.heliyon.2018.e00554

[21] R. Matsuzaki, M. Shiota, Data assimilation for three-dimensional flow monitoring in non-flat composite structures during vacuum-assisted resin transfer molding: a numerical study, Compos. Struct. 172 (2017) 155−165.

[22] M. Harsch, J. Karger-Kocsis, M. Holst, Influence of fillers and additives on the cure kinetics of an epoxy/anhydride resin, Eur. Polym. J. 43 (4) (2007) 1168−1178.

[23] H.C. Park, N.S. Goo, K.J. Min, K.J. Yoon, Three-dimensional cure simulation of composite structures by the finite element method, Compos. Struct. 62 (1) (2003) 51−57.

[24] J. Crank, P. Nicolson, A practical method for numerical evaluation of solutions of partial differential equations of the heat-conduction type, in: Mathematical Proceedings of the Cambridge Philosophical Society, 1947, pp. 50−67.

[25] X. Yang, T. Delsole, Using the ensemble Kalman filter to estimate multiplicative model parameters, Tellus A 61 (5) (2009) 601−609.

[26] Z. Guo, S. Du, B. Zhang, Temperature field of thick thermoset composite laminates during cure process, Compos. Sci. Technol. 65 (3-4) (2005) 517−523.

[27] D.C. Blest, B.R. Duffy, S. McKee, A.K. Zulkifle, Curing simulation of thermoset composites, Compos. Appl. Sci. Manuf. 30 (11) (1999) 1289−1309.

https://doi.org/10.1016/j.heliyon.2018.e00554